High-Resolution Manganese-Enhanced MRI of Experimental Retinopathy of Prematurity

Bruce A. Berkowitz,[1,2] *Robin Roberts,*[1] *John S. Penn,*[3] *and Marius Gradianu*[1]

Purpose. To test the hypothesis that in experimental retinopathy of prematurity (ROP), retinal neovascularization (NV) and vessel tortuosity have distinct spatial and temporal links with receptor and postreceptor ion demand.

Methods. Newborn rats were raised in either room air (controls) or variable oxygen (50%/10% [50/10]). After 14 days, 50/10 rats were recovered in room air until postnatal day (P) 19 or P22. Peripheral retinal NV severity and incidence and panretinal arteriole and venule tortuosity indexes (TI_a, TI_v) were measured from ADPase-stained retinal wholemounts. Intraretinal ion demand and retinal thickness were measured from high-resolution manganese-enhanced MRI (MEMRI). In separate experiments, intraretinal manganese uptake was also measured in adult rats pretreated with diltiazem, a Ca^{2+} channel antagonist.

Results. In 50/10 rats, peripheral retinal NV severity was significantly greater than in controls at P19 and was decreased by P22. Panretinal TI_a and TI_v were increased over control values at P19, but only TI_v decreased by P22. Unlike control retinas at P19 that had a centroperipheral total retinal thickness gradient, 50/10 retinas had similar central and peripheral total retinal thickness. The 50/10 group also demonstrated a correlation between peripheral retinal NV and TI_a and TI_v. Peripheral intraretinal uptake of manganese was significantly supernormal at P19 and decreased by P22. Increased peripheral intraretinal retinal manganese uptake was associated with peripheral NV severity and panretinal TI_a. In contrast, ion demand of central postreceptor, but not receptor, retina was significantly associated with peripheral NV severity and panretinal TI_a. Panretinal TI_v was not correlated with intraretinal ion demand in any case. In adult rats, diltiazem suppressed ($P < 0.05$) intraretinal manganese uptake.

Conclusions. The present data raise the possibility that altered retinal layer-specific ion demand causes retinal circulation abnormalities in experimental ROP. (*Invest Ophthalmol Vis Sci.* 2007;48:4733–4740) DOI:10.1167/iovs.06-1516

From the [1]Department of Anatomy and Cell Biology and the [2]Department of Ophthalmology, Wayne State University, Detroit, Michigan; and the [3]Vanderbilt Eye Institute, Vanderbilt University School of Medicine, Nashville, Tennessee.

Supported by National Institutes of Health Grants EY013831 (BAB) and EY07533 (JSP), the Juvenile Diabetes Research Foundation (BAB), a Research to Prevent Blindness Senior Scientific Investigator Award (JSP), and an unrestricted grant from Research to Prevent Blindness (BAB).

Submitted for publication December 20, 2006; revised April 26, 2007; accepted August 13, 2007.

Disclosure: **B.A. Berkowitz**, None; **R. Roberts**, None; **J.S. Penn**, None; **M. Gradianu**, None

The publication costs of this article were defrayed in part by page charge payment. This article must therefore be marked "*advertisement*" in accordance with 18 U.S.C. §1734 solely to indicate this fact.

Corresponding author: Bruce A. Berkowitz, Department of Anatomy and Cell Biology, Wayne State University School of Medicine, 540 E. Canfield, Detroit, MI 48201; baberko@med.wayne.edu.

Retinopathy of prematurity (ROP) is considered a vascular disease because it can manifest with tortuous retinal blood vessels and because blinding complications are associated with focal proliferation of the peripheral retinal circulation through the inner limiting membrane into the vitreous humor (neovascularization [NV]). However, preclinical and clinical ROP also demonstrate receptor (layers of the outer retina: inner and outer segments of the photoreceptor, outer nuclear layer, and outer plexiform layer) and postreceptor (layers of the inner retina: inner nuclear layer, inner plexiform layer, and ganglion cell layer) deficits on electroretinography (ERG).[1–3] To date it has not been possible to determine whether retinal dysfunction is spatially and temporally correlated with NV severity. One reason for this knowledge gap is that ERG responses to full-field stimuli used in ROP studies measures a spatially integrated response that cannot be correlated with focal NV in the peripheral retina. Evidence that both receptor and postreceptor retina may play roles in the development of retinal NV includes a report that NV was nearly undetectable in mice with inherited photoreceptor degeneration exposed to an oxygenation procedure that produces substantial preretinal NV in normal mice.[4] These results are intriguing but do not clearly demonstrate a role for intact neural retina in the development of retinal NV.

Normal retinal function, including photoreceptor transduction, retinal neuronal transmitter release, regulation of gap-junction conductance, and modulation of postsynaptic potentials in retinal ganglion cells, is strongly dependent on proper cellular demand for ions such as calcium. In addition, ionic control is important in the cell cycle and in neuronal development, and ion demand has been used as an index of viability in proliferating cells.[5–7] Experimentally induced acidosis in infant rats is associated with retinal NV, suggesting a link between perturbed ion homeostasis and preretinal NV, though a spatial association could not be tested with those data.[8,9] Thus, cellular demand for ions appears to be a reasonable biomarker of normal and abnormal retinal activity.

We used systemically administered $MnCl_2$ as a probe of layer-specific retinal ion demand in vivo. Manganese ion (Mn^{2+}) is a surrogate for ions such as calcium,[10] an essential trace element,[11] and a strong MRI contrast agent.[10] In rats in vivo, manganese-enhanced MRI (MEMRI) robustly measures with high spatial resolution manganese uptake in two dimensions: in different retinal layers and from these layers as they span panretinally from ora serrata to ora serrata. In addition, MEMRI data are strongly linked with normal and abnormal retinal activity.[12,13] In this study, we tested the hypothesis that in an experimental ROP model, retinal vascular abnormalities (NV and tortuosity) have distinct spatial and temporal links with receptor and postreceptor ion demand, as assessed with MEMRI.

Methods

Animals were treated in accordance with the National Institutes of Health Guide for the Care and Use of Laboratory Animals and the ARVO Statement for the Use of Animals in Ophthalmic and Vision Research.

TABLE 1. Summary of ADPase-Derived Retinal Vascular Parameters

Group	Subjects (*n*)	NV		TI	
		Incidence (%)	Severity Median (Range)	Arteriole (AU)	Venule (AU)
C P19	14	0	—	1.075 ± 0.005	1.069 ± 0.005
50/10 P19	8	100*	10 (8–2)	1.190 ± 0.025*	1.115 ± 0.078*,†
50/10 P22	5	100*	6 (5–7)‡	1.162 ± 0.013*	1.100 ± 0.006*,†

Severity is expressed in clock hours. TI values are expressed as mean ± SEM.
* $P < 0.05$, compared with C P19.
† $P < 0.05$, compared with TI arteriole (TI_a).
‡ $P < 0.05$, compared with 50/10 P19.

Assessment of Retinal Vascular Abnormality

ROP Model. The newborn rat model of ROP has been described in detail elsewhere and was performed in the laboratory of JSP. Briefly, Sprague-Dawley mothers and litters (12–15 pups per litter) were housed in a modified pediatric incubator in which the oxygen levels were varied between 50% and 10% (50/10) every 24 hours until postnatal day (P) 14. Rats were then allowed to recover in room air. At P17, dams and infant rats were flown to the laboratory of BAB, and different subsets of animals were studied on P18 ($n = 2$), P19 ($n = 6$), and P22 ($n = 5$). Because no difference in NV incidence and severity was found between P18 and P19 time points (data not shown), these two groups were combined. The combined data were weighted toward the P19 group and are identified as P19. In addition, separate groups of control rat pups were maintained in the laboratory of BAB in room air until P7 (to study peripheral intraretinal ion demand in retinas vascularized as were P19 50/10 rats) or P19 (age-matched controls). All rats were housed and maintained in normal 12-hour cycled laboratory lighting. Dams and pups were maintained in darkness overnight and then were light adapted for 20 minutes before $MnCl_2$ injection. $MnCl_2$ was administered as an intraperitoneal injection (44 mg/kg) on the right side of P18 ($n = 2$), P19 ($n = 4$), and P22 ($n = 5$) awake rats. Note that one P22 pup was excluded from the final analysis because the thickness of its peripheral retina was approximately 50% lower ($P < 0.05$) than that of the other pups in the group (mean, 237 mm; see Table 2). Thus, only four P22 rats were included in the final analysis. In addition, two P19 rats were not injected with $MnCl_2$ and were used as negative controls. Rats were maintained in light conditions for another 3.5 hours and then underwent anesthesia for MEMRI evaluation. After the MEMRI examination, infant rats were killed with an intracardiac potassium chloride injection, both eyes were enucleated, and retinas were wholemounted for staining and analysis.

Wholemount Analysis. Adenosine diphosphatase (ADPase)–stained wholemounts of all infant rats were analyzed, as previously described, to determine retinal NV incidence and severity and vessel tortuosity.[1,14,15] To determine NV severity, two investigators independently scored each wholemount in clock hours of NV in a masked fashion, and, for each retina, the median of these two scores was calculated. To determine severity of NV, the number of clock hours (score 0–12) occupied by abnormal vessel growth was determined.

To measure tortuosity, we analyzed stained wholemounts (instead of fluorescein angiograms) and assigned a tortuosity index (TI) for arterioles and venules, as described by Liu et al.[1] Briefly, a fixed circular region of interest centered on the optic nerve was used. For each blood vessel, TI was calculated as the ratio of the actual length (AL) to the straight-line length (SL) of a blood vessel using NIH IMAGE (a freeware program available at http://rsb.info.nih.gov/nih-image/; last accessed 5/12/04; developed by Wayne Rasband, National Institutes of Health, Bethesda, MD). Mean TI for the arterioles (TI_A) and for the venules (TI_V) in each wholemount was determined.

Adult Rat Diltiazem Experiment. Adult Sprague-Dawley female rats (196–223 g) were either untreated ($n = 4$) or treated with 5 mg/kg body weight diltiazem ($n = 5$) or 30 mg/kg body weight diltiazem ($n = 4$) intraperitoneally at least 30 minutes before administration of the manganese. $MnCl_2$ dose and timing were the same as described.

MRI Data Acquisition

High-Resolution MRI. Immediately before the MRI experiment, adult and newborn rats were anesthetized with urethane (36% solution administered intraperitoneally, 0.083 mL/20 g animal weight, prepared fresh daily; Aldrich, Milwaukee, WI). To maintain the core temperature, a recirculating heated water blanket was used. Rectal temperatures were continuously monitored throughout each experiment, as previously described.[16] MRI data were acquired on a 4.7-T nuclear magnetic resonance analysis system (Avance; Bruker, Billerica, MA) using a two-turn transmit/receive surface coil (1-cm diameter) placed over the left eye. On sagittal localizer images collected with the same adiabatic pulse sequence described, a single transverse slice positioned in the middle of the lens and the middle of the optic nerve (through the center of the eye) was chosen. Images were acquired using an adiabatic spin-echo imaging sequence (repetition time [TR], 350 seconds; echo time [TE], 16.7 ms; number of acquisitions [NA], 16; sweep width, 61,728 Hz; matrix size, 256 × 512; slice thickness, 620 μm; field of view, 12 × 12 mm^2; 23 minutes/image).[17] Different phase-encoding directions were used to provide 23.4 μm intraretinal resolution for central (AP encoding) and peripheral (LR encoding) retina.

MRI Data Analysis. Signal intensities of postreceptor and receptor retina and total and postreceptor retinal thicknesses were analyzed from 1 pixel–thick regions at two locations: in central retina (0.4–1 mm from the optic nerve) and in peripheral retina (1 mm on either side of the mean distance at which NV develops (2.75 mm from the optic nerve).

Retinal Thickness. As previously described and validated against histology, on each image, inner or total retinal thicknesses were measured, respectively, as the radial distance between the anterior edge and the middle edge (defined by its change in signal intensity) or the posterior edge of the retina at distances ±0.4 to 1 mm from the optic nerve.[12] Mean superior and inferior values generated for each rat were used for comparisons. In several rats, an artifact was noted on the peripheral inferior retina that appeared to be caused by slightly off-center coil placement (see Fig. 2); hence, only peripheral superior retina data are reported.

Layer-Specific Signal Intensity. For visualization and comparison purposes, in-house written software was used to map the in situ image into a linear representation for each retina. The vitreoretinal border and optic nerve were manually defined. Using the center point of each highlighted pixel, a straight line was fit to the optic nerve, and a sixth-order polynomial was fit to the vitreoretinal border. The intercept between the vitreoretinal border and the optic nerve regions-of-interest served as the origin of the linearized image. Along the polynomial, 50,000 evenly spaced values were then chosen by the program, and distances between each point and the one adjacent were calculated. Using these distance measurements, fine-grained linear ap-

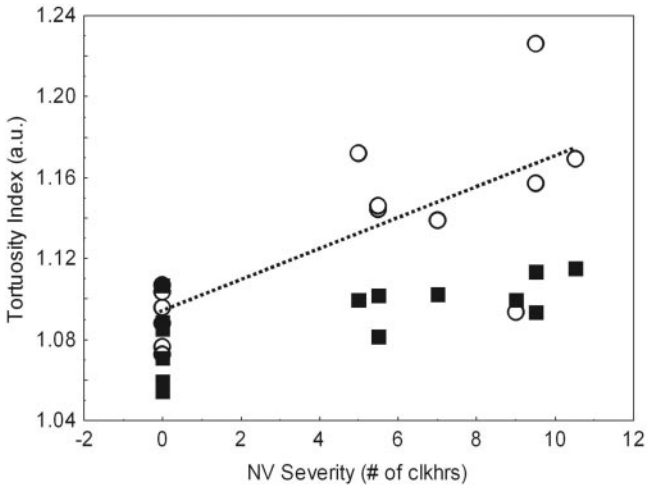

FIGURE 1. Plot of TI_a (○) and TI_v (■) versus NV severity. Data points are from separate animals. *Dotted line* is only shown for correlated data and represent best fit to a linear equation for TI_a ($r = 0.7$; $P = 0.002$). Because of large scatter in TI_v values in retinas without NV, correlation analysis was not performed. The data at the origin of the *x*-axis represented is from control rats.

proximations of distances along the polynomial were available. For each of the 50,000 values, a line normal to every fiftieth was drawn and intensity values along the normal were extracted and reconstructed into the linearized image. Within each group, linearized retinas were averaged into a composite image for visual comparisons between groups. For quantitative analysis, postreceptor and receptor retinal signal intensities for each rat were determined and then analyzed using the program IMAGE and derived macros.[12] Signal intensities from each retinal layer were analyzed using the NIH IMAGE program and derived macros.[18] Changes in receiver gain between animals were controlled for by setting the signal intensity of a fixed region of noise in each rat to a fixed value. Other tissues within the sensitive volume of the coil demonstrated enhancement after manganese injection and were considered inadequate as internal references. The border between postreceptor and receptor retina was set at 4 pixels (93.6 μm) posterior to the clearly defined vitreoretinal division. We set the border of retina and choroid at 3 pixels (70.2 μm) posterior from postreceptor/receptor division (receptor division). Pixels immediately anterior to the postreceptor and receptor borders were considered representative of postreceptor and receptor retina, respectively, and were analyzed as previously described.[12]

Statistical Analysis. To compare TI, an unpaired 2-tailed *t*-test analysis was used. To compare the NV severity (in clock hours), a two-sample Mann-Whitney rank sum test (2-sided) was used. The Mann-Whitney test is the statistical analysis most appropriate for comparisons of two nonparametric data sets. Because the scale used to generate them is limited to whole numbers, the clock hour data are nonparametric. To compare NV incidence, a 2×2 χ^2 test was performed. Retinal thickness data were compared using an unpaired 2-tailed *t*-test analysis. Comparisons of MEMRI retinal signal intensities were performed using a generalized estimating equation (GEE) approach.[19] GEE performs general linear regression analysis using all the pixels in each subject and accounts for the within-subject correlation between adjacent pixels. Unless otherwise noted, two-tailed $P < 0.05$ was considered statistically significant.

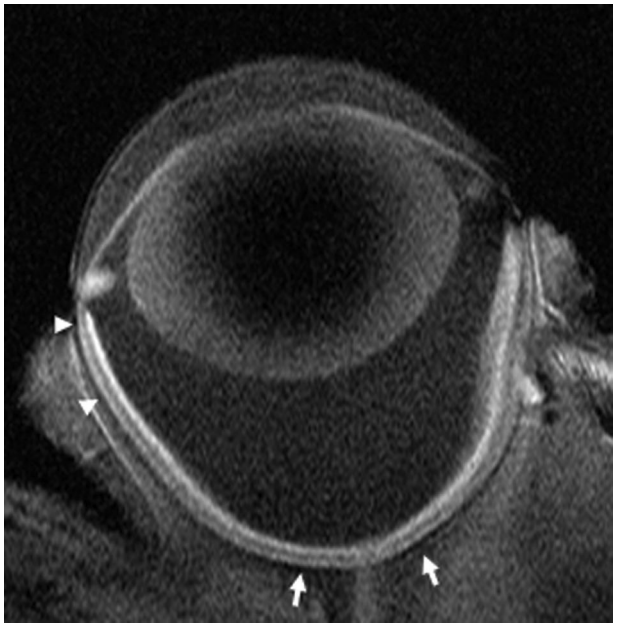

FIGURE 2. Representative high-resolution MEMRI data of a P19 50/10 pup illustrating the regions of the eye that were analyzed in this study. *White arrows*: central region. *White arrowheads*: peripheral region.

RESULTS

Wholemount Analysis

A summary of preretinal peripheral retinal NV incidence and severity at days P19 and P22 is presented in Table 1. As expected, peripheral retinal NV incidence and severity at P19 were greater ($P < 0.05$) than age-matched controls.[20] The severity of the peripheral retinal NV was also greater ($P < 0.05$) at P19 than at P22.[20] Panretinal TI_A and TI_V are summarized in Table 1. At P19 and P22, mean panretinal TI_A and TI_v for the experimental ROP group were greater ($P < 0.05$) than the age-matched control group. However, TI_v, but not TI_a, at P19 was different ($P < 0.05$) from those measured at P22. In addition, as shown in Figure 1, panretinal arteriole TI and NV were correlated ($r = 0.7$; $P = 0.002$).

MEMRI

Retinal Thickness. At P19, control, but not experimental, rats demonstrated different ($P < 0.05$) total retinal thicknesses

TABLE 2. Summary of MRI-Derived Retinal Thicknesses

Group	Subjects (*n*)	Total Thickness (μm)		Postreceptor (μm)	
		Central	Peripheral	Central	Peripheral
C P19	6	243.2 ± 4.8	223.1 ± 5.0*	103.5 ± 3.0	97.8 ± 4.7
50/10 P19	6	235.3 ± 4.3	231.9 ± 6.4	100.3 ± 2.4	108.4 ± 4.9
50/10 P22	4	—	236.8 ± 4.1	—	105.1 ± 5.9

Values are expressed as mean ± SEM.
* $P < 0.05$; compared with C P19 central retinal thickness.

between central and peripheral retina (Table 2). No differences ($P > 0.05$) were found in central and peripheral total or postreceptor thickness between groups (Table 2).

Intraretinal Signal Intensities. Mean linearized images were generated from the region of peripheral retina (Fig. 2) that developed retinal NV (2.75 ± 0.04 mm from the optic nerve, dotted circle overlaid on the wholemount in Fig. 3) for P19 control and 50/10 groups and for the P22 rats (Fig. 3). Visual inspection of Figure 3 suggests that peripheral retinal ion demand was increased intraretinally at P19 and then decreased by P22. Quantitative analysis confirmed that manganese uptake in peripheral postreceptor and receptor retina was supernormal ($P < 0.05$) relative to age-matched controls (Fig. 3) and in control rats with a similar extent of vascular development (P7 control rats, 2.8–2.9 mm from the optic nerve head; Fig. 3). In addition, central intraretinal ion demand was supernormal (Figs. 2, 4). Peripheral and central retinal ion demand changed differently for age-matched control and 50/10 rats (Fig. 5). In the 50/10 group at P22 (during regression of NV), postreceptor and receptor signal intensities were significantly ($P < 0.05$) lower than their values at P19 (Fig. 3).

Comparison of Retinal Vascular Parameters and Intraretinal Signal Intensities. As summarized in Figures 6 and 7, peripheral and central postreceptor retinal signal intensity were associated with peripheral retinal NV severity ($r = 0.5$, $P = 0.06$, and $r = 0.8$, $P = 0.02$, respectively) and panretinal

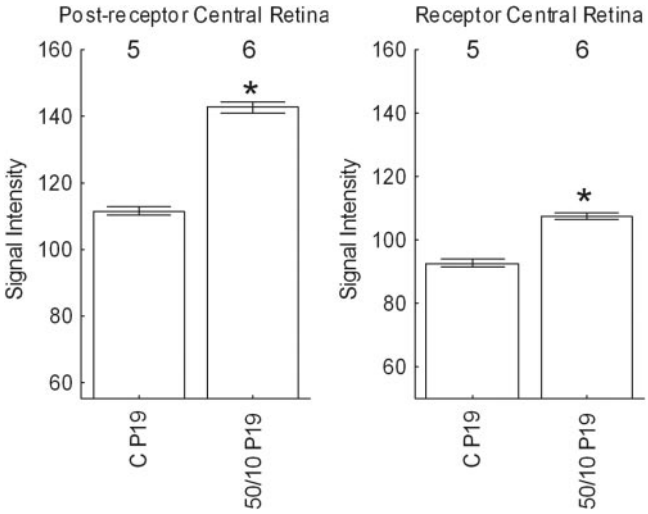

Figure 4. MEMRI signal intensity (arbitrary units) changes in central postreceptor and receptor retina in C P19, and 50/10 P19 light-adapted rats measured 4 hours after intraperitoneal systemic administration of $MnCl_2$. Significant differences ($^*P < 0.05$) are noted. Note that the minimum value (55) of the *x*-axis is set to signal intensity measured in the absence of manganese exposure.[12] Error bars represent SEM, and numbers above the bars represent number of animals studied.

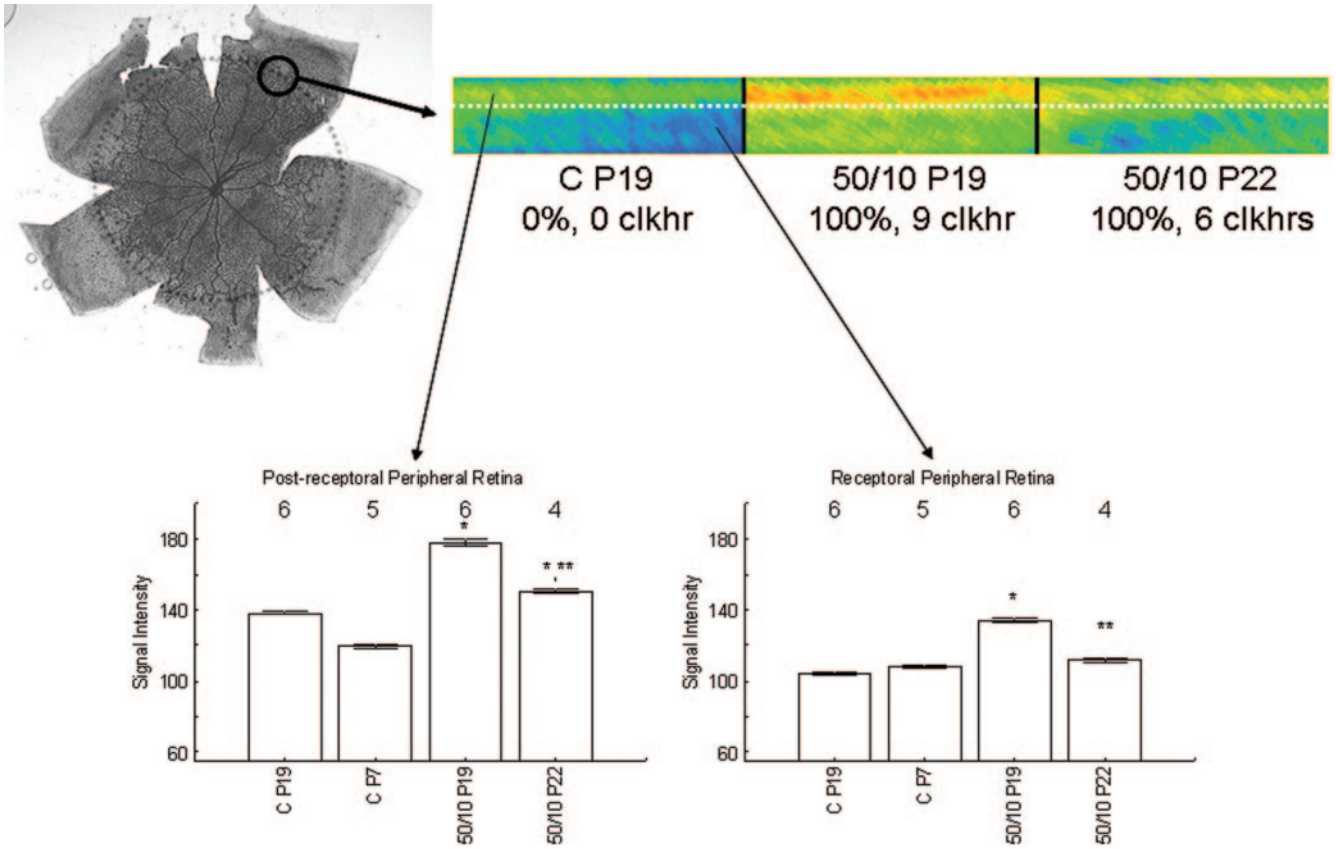

Figure 3. *Top left:* representative ADPase-stained retinal wholemount from a P19 50/10 pup. *Dotted line*: average distance of retinal vessel edge from the optic nerve (2.75 ± 0.04 mm from the optic nerve). Mean linearized pseudocolor images (*top right*) of age-matched controls (C P19), 50/10 pups at P19 (50/10 P19), and 50/10 pups at P22 (50/10 P22) were derived from this peripheral region of superior retina. The same pseudocolor scale was used for all three linearized images, where *blue* to *green* to *yellow* to *red* represent lowest to highest signal intensity. *Dotted white line*: boundary between postreceptor and receptor retina of the control retinas demonstrated in previous studies.[12,21] *Bottom*: MEMRI signal intensity (arbitrary units) changes in peripheral postreceptor (*left*) and receptor (*right*) retina in C P19, C P7 (to study peripheral intraretinal ion demand in retinas vascularized to a similar degree as P19 50/10 rats), 50/10 P19, and 50/10 P22 light-adapted rats measured 4 hours after intraperitoneal systemic administration of $MnCl_2$. Significant differences ($^*P < 0.05$) are noted. Note that the minimum value (55) of the *x*-axis is set to signal intensity measured in the absence of manganese exposure.[12] Error bars represent SEM, and numbers above the bars represent number of animals studied.

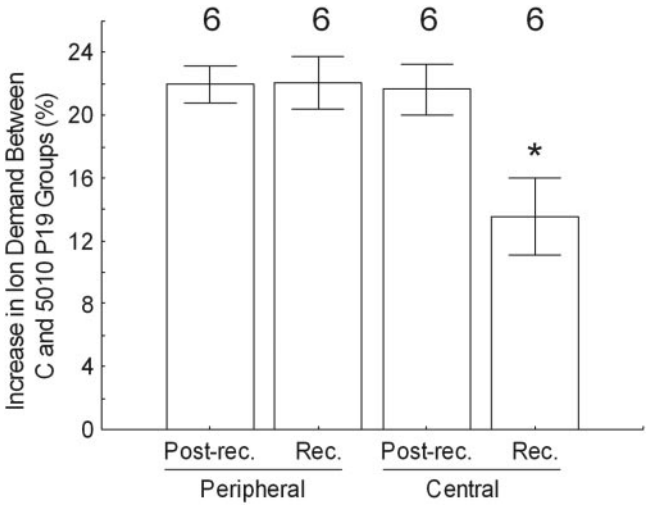

FIGURE 5. Percentage change of signal intensity (arbitrary units) between age-matched control (C) and 50/10 groups at P19 for peripheral and central postreceptor (Postrec.) and receptor (Rec.) retina. Error bars represent SEM, and numbers above the bars represent number of animals studied.

TI_a ($r = 0.7$, $P = 0.01$, and $r = 0.7$, $P = 0.03$). Central receptor uptake of manganese did not correlate with retinal NV or TI_a. Panretinal TI_v did not correlate with intraretinal ion demand in any case.

Adult Rat Diltiazem Experiment. In adult rats, diltiazem treatment significantly reduced ($P < 0.05$) intraretinal manganese uptake relative to controls in a dose-dependent manner (Fig. 8).

DISCUSSION

The major results of this study are that TI_a was correlated with peripheral retinal NV severity in the experimental ROP model (Fig. 2), that peripheral retinal NV severity was associated spatially and temporally with supernormal ion demand in receptor and postreceptor portions of the peripheral retina (Figs. 3, 6), and that panretinal TI_a was spatially and temporally correlated with supernormal intraretinal ion demand (Figs. 3, 5, 6). The present findings are consistent with previous findings in experimental ROP of significant vascular and neural abnormalities.[1,22–28] Neuronal dysfunction in ROP rats had previously been assessed by ERG. However, because ERG cannot be used to measure differential centroperipheral responses, detailed comparisons with the present results are not possible.[1,24–28] These results highlight MEMRI as a powerful approach for robustly studying focal changes in retinal physiology and pathophysiology in vivo.[12]

ROP is generally characterized by two vascular abnormalities, retinal vessel tortuosity and retinal NV.[29] Vessel tortuosity is a commonly used as a clinical indicator of risk for progression to more severe ROP, including retinal NV, and as a guide for determining when to intervene with treatment.[30] Only one report to our knowledge, by Liu et al.,[1] has quantitatively measured vessel tortuosity in this model, though their study did not look for a correlation between tortuosity and retinal NV. The infant rat model used in this study has been extensively tested and robustly produces retinal NV with 100% incidence and 6 to 8 clock hour severity.[22,31] We find that TI_a was greater than TI_v (Table 2), consistent with the data of Liu et al.[1] Our data extend the work of Liu et al.[1] by demonstrating for the first time in this infant rat model of ROP that TI_a and TI_v are correlated with NV severity. In addition, we report that receptor and postreceptor portions of the peripheral retina were also spatially and temporally linked with retinal NV severity and TI_a, but not TI_v. At present, it is unclear why venule tortuosity did not correlate with intraretinal ion demand, though the reason may be related more to the sensitivity of the different techniques used than to lack of a biological association.

In this study, we found evidence that the normal centroperipheral gradient of total retinal thickness[32] was abnormal at P19 in the experimental ROP model. No changes in inner retinal thickness were noted in any of the groups (Table 2). The thickness changes in Table 2 were smaller than the pixel size; some caution is needed when interpreting such differences. Nonetheless, there is evidence that oxygen exposure in newborn rats can alter retinal thickness.[33] Thus, it is plausible that the apparent decrease in centroperipheral thickness gradient in this ROP model is real.

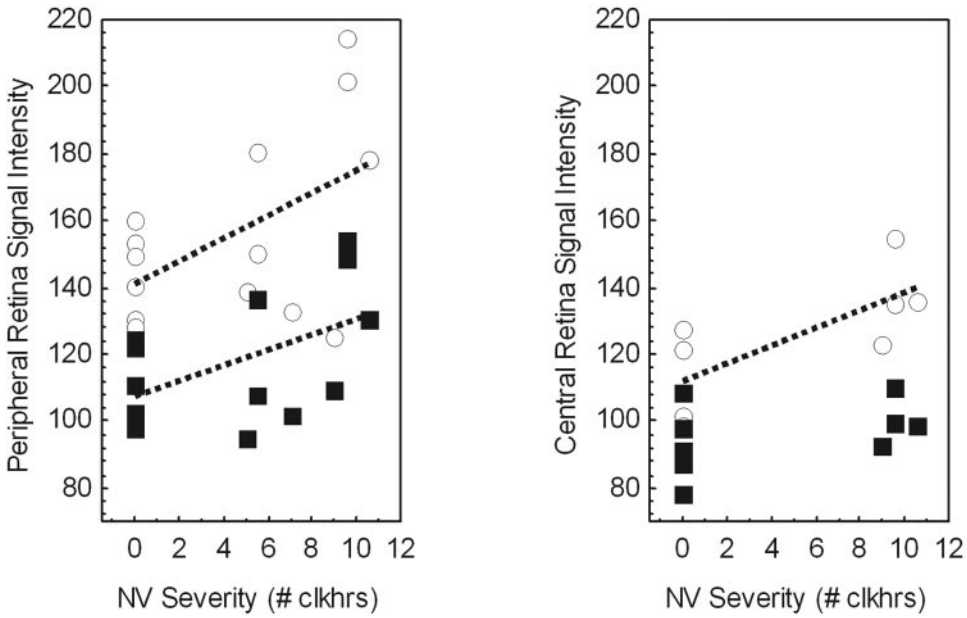

FIGURE 6. Plot of peripheral (*left*) and central (*right*) postreceptor (○) and receptor (■) retina signal intensity (arbitrary units) compared with NV severity. Data points are from separate animals in all groups (C P19, P19, P22). *Dotted lines*: correlated or nearly correlated data, representing best fit to a linear equation for peripheral postreceptor ($r = 0.5$; $P = 0.057$) and receptor ($r = 0.5$; $P = 0.059$) regions and central postreceptor ($r = 0.8$; $P = 0.018$) and receptor ($r = 0.4$; $P = 0.29$) retina. Statistical significance is reported for two-tailed analysis. Note that MEMRI data for measuring central retinal signal intensities were not collected in the P22 group, resulting in fewer data points for this graph.

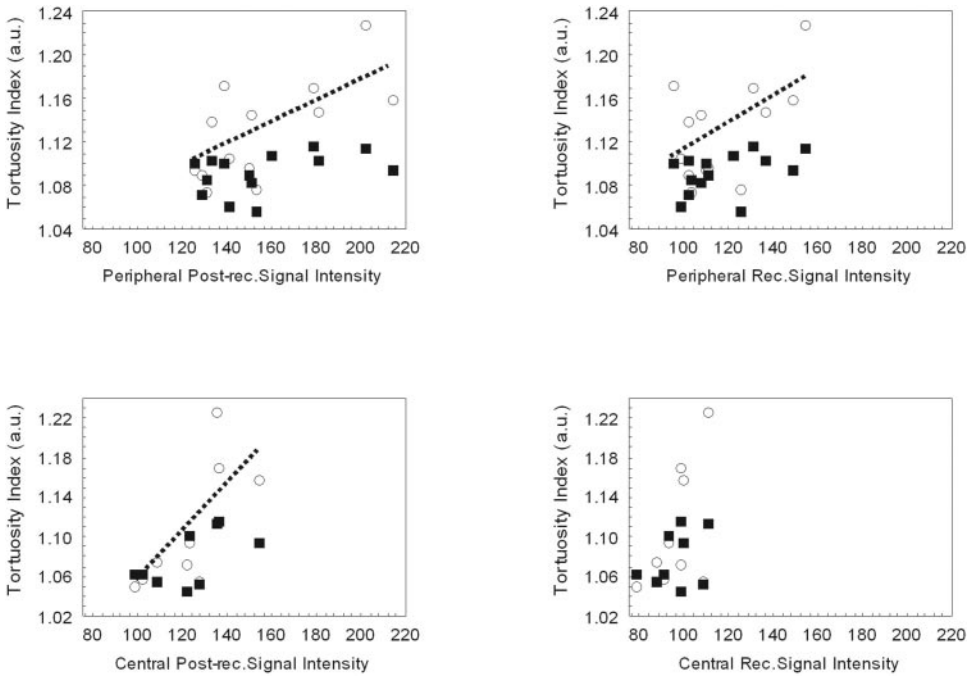

FIGURE 7. Plot of peripheral (*top row*) and central (*bottom row*) TI_a (○) and TI_v (■) versus retina signal intensity (arbitrary units). Data points are from separate animals in all groups (C P19, P19, P22). *Dotted lines*: correlated data, representing best fit to a linear equation for peripheral postreceptor ($r = 0.7$; $P = 0.009$) and receptor ($r = 0.4$; $P = 0.158$) regions, peripheral receptor ($r = 0.5$; $P = 0.042$) and receptor ($r = 0.4$; $P = 0.142$) regions, central postreceptor ($r = 0.7$; $P = 0.027$) and receptor ($r = 0.6$; $P = 0.082$) regions, and central receptor ($r = 0.6$; $P = 0.107$) and receptor ($r = 0.3$; $P = 0.363$) regions. Statistical significance is reported for two-tailed analysis.

The mechanism responsible for an increase in intraretinal manganese uptake in the ROP pups is unknown. Manganese is extensively bound to plasma proteins, and it is possible that control and ROP pups had dissimilar plasma protein levels.[34] However, comparable plasma protein levels have been reported in newborn rat groups, similar to those in this study.[35] Another possibility is that differences in manganese-bound protein uptake into the retina, and not manganese ion, are measured by MEMRI. One approach for testing this hypothesis could involve comparing intraretinal signal intensities in the newborn rat NV model with and without treatment of a calcium channel antagonist (e.g., diltiazem). Based on the literature, however, diltiazem treatment reduces NV severity.[36] Given that the present data finds evidence for an association between retinal NV and manganese uptake, interpretation of the results of this calcium channel antagonist experiment is difficult. Nonetheless, in this study, we did confirm that prophylactic systemic treatment of adult rats with diltiazem at doses expected to block Ca^{2+} channel activity[37] substantially inhibited Mn^{2+} entry into activated retinal cells (Fig. 8). A related hypothesis is that transport of free or plasma protein-bound manganese through the blood-retinal barrier (BRB) or leaky intracameral uveal vessels associated with immature or damaged retinas may be different in the two newborn rat groups, and this difference could modulate intraretinal signal intensity.[35] This supposition does not seem supported by previous data in adult rats in which increased BRB permeability was not a likely explanation for increased intraretinal signal intensities after retinal injury.[13] We also noted that development of the retinal and hyaloidal circulations was similar in control P7 and 50/10 P19 groups. These considerations are not consistent with a regulatory role of protein-bound manganese, BRB damage, or immature intracameral uveal vessels in the present findings.

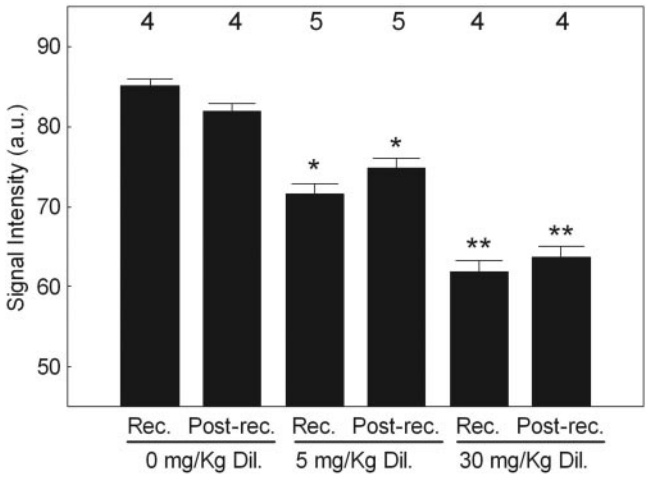

FIGURE 8. Comparison of intraretinal signal intensities in nontreated rats (0 mg/kg Dil.) and rats treated with two different doses of the Ca^{2+} channel antagonist diltiazem in adult rats (5 mg/kg Dil., 30 mg/kg Dil.). Dark-adapted MEMRI signal was progressively ($P < 0.5$) suppressed with increasing doses of diltiazem. Error bars represent SEM, and numbers above the bars represent number of animals studied.

An alternative explanation is that the supernormal manganese uptake in the 50/10 group represented increased intraretinal ion demand. In the retina, we found agreement between changes in intraretinal manganese uptake and conditions that would be expected to alter ion demand, such as light/dark adaptation, suppressed Na/K-ATPase activity, retinal injury, and calcium channel antagonism (Fig. 8).[12,13] These considerations are consistent with evidence in other tissues that avid uptake occurs through channels for ions, such as calcium in which channel affinity for Mn^{2+} is high despite extensive binding to plasma proteins, which lowers the extracellular availability of free manganese ions.[34] In further support of this ion demand hypothesis, we note that in control infant rats, systemic acidosis and alkalosis, conditions expected to alter intraretinal ion homeostasis,[38,39] are associated with preretinal NV.[8,9,40] Furthermore, a drug treatment that causes intraretinal acidification has also been shown to cause an increase in intraretinal manganese uptake.[13,41] More work is needed to better understand the mechanism responsible for manganese uptake. Nonetheless, these considerations are consistent with

our premise of a link between retinal layer-specific ion demand and retinal NV.

Temporal and spatial correlations between different retinal layers and vascular abnormalities are reported herein for the first time. It has been noted that the developmental age during which vascular abnormalities associated with ROP are apparent corresponds to when substantial changes occur in receptor (e.g., rapid rod outer segment elongation, increasing rhodopsin content of the retina, and escalating energy demands[1]) and postreceptor retina (e.g., extensive dendritic differentiation and remodeling[42–44]). These developmental changes depend on proper intraretinal ion demand. Work is ongoing in our laboratory to refine our understanding of these links by determining whether ion dyshomeostasis occurs in dark-adapted retinas, before the appearance of retinal NV, and in other retinal NV models. Nonetheless, consideration of the present results, together with previous work by Holmes et al.,[8,9,40] raises the possibility that altered retinal layer-specific ion demand causes retinal circulation abnormalities in ROP.

Acknowledgments

The authors thank Anne Fulton for the many clarifying comments.

References

1. Liu K, Akula JD, Falk C, Hansen RM, Fulton AB. The retinal vasculature and function of the neural retina in a rat model of retinopathy of prematurity. *Invest Ophthalmol Vis Sci*. 2006;47(6):2639–2647.
2. Fulton AB, Hansen RM, Petersen RA, Vanderveen DK. The rod photoreceptors in retinopathy of prematurity: an electroretinographic study. *Arch Ophthalmol*. 2001;119(4):499–505.
3. Reynaud X, Hansen RM, Fulton AB. Effect of prior oxygen exposure on the electroretinographic responses of infant rats. *Invest Ophthalmol Vis Sci*. 1995;36(10):2071–2079.
4. Lahdenranta J, Pasqualini R, Schlingemann RO, et al. An antiangiogenic state in mice and humans with retinal photoreceptor cell degeneration. *Proc Natl Acad Sci USA*. 2001;98(18):10368–10373.
5. Tamano H, Enomoto S, Oku N, Takeda A. Preferential uptake of zinc, manganese, and rubidium in rat brain tumor. *Nucl Med Biol*. 2002;29(4):505–508.
6. Young TL, Cepko CL. A role for ligand-gated ion channels in rod photoreceptor development. *Neuron*. 2004;41(6):867–879.
7. Santella L, Ercolano E, Nusco GA. The cell cycle: a new entry in the field of $Ca2^{+}$ signaling. *Cell Mol Life Sci*. 2005;62(21):2405–2413.
8. Zhang S, Leske DA, Lanier WL, Berkowitz BA, Holmes JM. Preretinal neovascularization associated with acetazolamide-induced systemic acidosis in the neonatal rat. *Invest Ophthalmol Vis Sci*. 2001;42(5):1066–1071.
9. Holmes JM, Zhang S, Leske DA, Lanier WL. Metabolic acidosis-induced retinopathy in the neonatal rat. *Invest Ophthalmol Vis Sci*. 1999;40(3):804–809.
10. Lin YJ, Koretsky AP. Manganese ion enhances T1-weighted MRI during brain activation: an approach to direct imaging of brain function. *Magn Reson Med*. 1997;38(3):378–388.
11. Gong H, Amemiya T. Ultrastructure of retina of manganese-deficient rats. *Invest Ophthalmol Vis Sci*. 1996;37(10):1967–1974.
12. Berkowitz BA, Roberts R, Goebel DJ, Luan H. Noninvasive and simultaneous imaging of layer-specific retinal functional adaptation by manganese-enhanced MRI. *Investe Ophthalmol Vis Sci*. 2006;47(6):2668–2674.
13. Berkowitz BA, Roberts R, Luan H, et al. Manganese-enhanced MRI studies of alterations of intraretinal ion demand in models of ocular injury. *Invest Ophthalmol Vis Sci*. 2007;48(8):3796–3804.
14. Berkowitz BA, Berlin ES, Zhang W. Variable supplemental oxygen during recovery does not reduce retinal neovascular severity in experimental ROP. *Curr Eye Res*. 2001;22(6):401–404.
15. Lutty GA, McLeod DS. A new technique for visualization of the human retinal vasculature. *Arch Ophthalmol*. 1992;110(2):267–276.
16. Berkowitz BA, Ito Y, Kern TS, McDonald C, Hawkins R. Correction of early subnormal superior hemiretinal ΔPO(2) predicts therapeutic efficacy in experimental diabetic retinopathy. *Invest Ophthalmol Vis Sci*. 2001;42(12):2964–2969.
17. Schupp DG, Merkle H, Ellermann JM, Ke Y, Garwood M. Localized detection of glioma glycolysis using edited 1H MRS. *Magn Reson Med*. 1993;30(1):18–27.
18. Berkowitz BA. Adult and newborn rat inner retinal oxygenation during carbogen and 100% oxygen breathing: comparison using magnetic resonance imaging delta PO_2 mapping. *Invest Ophthalmol Vis Sci*. 1996;37(10):2089–2098.
19. Liang Z. Longitudinal data analysis using generalized linear models. *Biometrika*. 1986;73:13–22.
20. Berkowitz BA, Zhang W. Significant reduction of the panretinal oxygenation response after 28% supplemental oxygen recovery in experimental ROP. *Invest Ophthalmol Vis Sci*. 2000;41(7):1925–1931.
21. Luan H, Roberts R, Sniegowski M, Goebel DJ, Berkowitz BA. Retinal thickness and subnormal retinal oxygenation response in experimental diabetic retinopathy. *Invest Ophthalmol Vis Sci*. 2006;47(1):320–328.
22. Penn JS, Henry MM, Tolman BL. Exposure to alternating hypoxia and hyperoxia causes severe proliferative retinopathy in the newborn rat. *Pediatr Res*. 1994;36(6):724–731.
23. Berkowitz BA, Penn JS. Abnormal panretinal response pattern to carbogen inhalation in experimental retinopathy of prematurity. *Invest Ophthalmol Vis Sci*. 1998;39(5):840–845.
24. Fulton AB, Hansen RM, Moskowitz A, Barnaby AM. Multifocal ERG in subjects with a history of retinopathy of prematurity. *Doc Ophthalmol*. 2005;111(1):7–13.
25. Fulton AB, Hansen RM, Petersen RA, Vanderveen DK. The rod photoreceptors in retinopathy of prematurity: an electroretinographic study. *Arch Ophthalmol*. 2001;119(4):499–505.
26. Fulton AB, Hansen RM. Photoreceptor function in infants and children with a history of mild retinopathy of prematurity. *J Opt Soc Am A*. 1996;13(3):566–571.
27. Reynaud X, Hansen RM, Fulton AB. Effect of prior oxygen exposure on the electroretinographic responses of infant rats. *Invest Ophthalmol Vis Sci*. 1995;36(10):2071–2079.
28. Penn JS, Thum LA, Rhem MN, Dell SJ. Effects of oxygen rearing on the electroretinogram and GFA-protein in the rat. *Invest Ophthalmol Vis Sci*. 1988;29(11):1623–1630.
29. Gelman R, Martinez-Perez ME, Vanderveen DK, Moskowitz A, Fulton AB. Diagnosis of plus disease in retinopathy of prematurity using Retinal Image multiScale Analysis. *Invest Ophthalmol Vis Sci*. 2005;46(12):4734–4738.
30. Saunders RA, Bluestein EC, Sinatra RB, Wilson ME, O'Neil JW, Rust PF. The predictive value of posterior pole vessels in retinopathy of prematurity. *J Pediatr Ophthalmol Strabismus*. 1995;32(2):82–85.
31. Zhang W, Ito Y, Berlin E, Roberts R, Luan H, Berkowitz BA. Specificity of subnormal ΔPO_2 for retinal neovascularization in experimental retinopathy of prematurity. *Invest Ophthalmol Vis Sci*. 200344(8):3551–3555.
32. Buttery RG, Hinrichsen CF, Weller WL, Haight JR. How thick should a retina be? A comparative study of mammalian species with and without intraretinal vasculature. *Vision Res*. 1991;31(2):169–187.
33. Dembinska O, Rojas LM, Varma DR, Chemtob S, Lachapelle P. Graded contribution of retinal maturation to the development of oxygen-induced retinopathy in rats. *Invest Ophthalmol Vis Sci*. 2001;42(5):1111–1118.
34. Nordhoy W, Anthonsen HW, Bruvold M, et al. Intracellular manganese ions provide strong T1 relaxation in rat myocardium. *Magn Reson Med*. 2004;52(3):506–514.
35. Berkowitz BA, Roberto KA, Penn JS. The vitreous protein concentration is increased prior to neovascularization in experimental ROP. *Curr Eye Res*. 1998;17(2):218–221.
36. Higgins RD, Yu K, Sanders RJ, Nandgaonkar BN, Rotschild T, Rifkin DB. Diltiazem reduces retinal neovascularization in a

mouse model of oxygen induced retinopathy. *Curr Eye Res*. 1999;18(1):20–27.

37. Lu H, Xi ZX, Gitajn L, Rea W, Yang Y, Stein EA. Cocaine-induced brain activation detected by dynamic manganese-enhanced magnetic resonance imaging (MEMRI). *Proc Natl Acad Sci USA*. 2007; 104(7):2489–2494.
38. Padnick-Silver L, Linsenmeier RA. Quantification of in vivo anaerobic metabolism in the normal cat retina through intraretinal pH measurements. *Vis Neurosci*. 2002;19(6):793–806.
39. Hiroi K, Yamamoto F, Honda Y. Analysis of electroretinogram during systemic hypercapnia with intraretinal K(+)-microelectrodes in cats. *Invest Ophthalmol Vis Sci*. 1994;35(11):3957–3961.
40. Berdahl JP, Leske DA, Fautsch MP, Lanier WL, Holmes JM. Effect of bicarbonate on retinal vasculature and acidosis-induced retinopathy in the neonatal rat. *Graefes Arch Clin Exp Ophthalmol*. 2005; 243(4):367–373.
41. Yamamoto F, Honda Y. Effects of intravenous iodoacetate and iodate on pH outside rod photoreceptors in the cat retina. *Invest Ophthalmol Vis Sci*. 1993;34(6):2009–2017.
42. Schmid S, Guenther E. Voltage-activated calcium currents in rat retinal ganglion cells in situ: changes during prenatal and postnatal development. *J Neurosci*. 1999;19(9):3486–3494.
43. Kalloniatis M, Tomisich G, Wellard JW, Foster LE. Mapping photoreceptor and postreceptoral labelling patterns using a channel permeable probe (agmatine) during development in the normal and RCS rat retina. *Vis Neurosci*. 2002;19(1):61–70.
44. Lohmann C, Wong RO. Regulation of dendritic growth and plasticity by local and global calcium dynamics. *Cell Calcium*. 2005; 37(5):403–409.